Small-molecule–directed, efficient generation of retinal pigment epithelium from human pluripotent stem cells

Julien Maruotti[a], Srinivas R. Sripathi[a], Kapil Bharti[b], John Fuller[a], Karl J. Wahlin[a], Vinod Ranganathan[a], Valentin M. Sluch[a], Cynthia A. Berlinicke[a], Janine Davis[b], Catherine Kim[a], Lijun Zhao[a], Jun Wan[a], Jiang Qian[a], Barbara Corneo[c], Sally Temple[d], Ramin Dubey[e,f], Bogdan Z. Olenyuk[g], Imran Bhutto[a], Gerard A. Lutty[a], and Donald J. Zack[a,h,i,j,1]

[a]Wilmer Eye Institute, Johns Hopkins University School of Medicine, Baltimore, MD 21287; [b]Unit on Ocular and Stem Cell Translational Research, National Eye Institute, National Institutes of Health, Bethesda, MD 20892; [c]Stem Cell Core Facility, Columbia University, New York, NY 10032; [d]Neural Stem Cell Institute, Rensselaer, NY 12144; [e]Department of Medicine, Stanford University School of Medicine, Stanford, CA 94305; [f]Department of Biochemistry, Stanford University School of Medicine, Stanford, CA 94305; [g]Department of Pharmacology and Pharmaceutical Sciences, University of Southern California, Los Angeles, CA 90089; [h]Department of Molecular Biology and Genetics, Johns Hopkins University, Baltimore, MD 21287; [i]Department of Neuroscience, Johns Hopkins University, Baltimore, MD 21287; and [j]Institute of Genetic Medicine, Johns Hopkins University School of Medicine, Baltimore, MD 21287

Edited by Jeremy Nathans, The Johns Hopkins University, Baltimore, MD, and approved July 17, 2015 (received for review December 1, 2014)

Age-related macular degeneration (AMD) is associated with dysfunction and death of retinal pigment epithelial (RPE) cells. Cell-based approaches using RPE-like cells derived from human pluripotent stem cells (hPSCs) are being developed for AMD treatment. However, most efficient RPE differentiation protocols rely on complex, stepwise treatments and addition of growth factors, whereas small-molecule–only approaches developed to date display reduced yields. To identify new compounds that promote RPE differentiation, we developed and performed a high-throughput quantitative PCR screen complemented by a novel orthogonal human induced pluripotent stem cell (hiPSC)-based RPE reporter assay. Chetomin, an inhibitor of hypoxia-inducible factors, was found to strongly increase RPE differentiation; combination with nicotinamide resulted in conversion of over one-half of the differentiating cells into RPE. Single passage of the whole culture yielded a highly pure hPSC-RPE cell population that displayed many of the morphological, molecular, and functional characteristics of native RPE.

retinal pigment epithelium | pluripotent stem cells | high-throughput screening | differentiation | age-related macular degeneration

Age-related macular degeneration (AMD) is the leading cause of irreversible vision loss and blindness among the elderly in industrialized countries. Dysfunction of the retinal pigment epithelium (RPE) is an early event associated with AMD. The RPE, a monolayer of pigmented cells directly abutting the photoreceptor cell layer, plays many important roles in vision and in maintaining the health and integrity of the retina (1). As the RPE deteriorates, there is progressive degeneration of photoreceptor cells.

Successful antiangiogenesis treatments have been developed for the neovascular, or "wet," form of AMD. However, there are no Food and Drug Administration-approved treatment options available for the majority of AMD patients, who suffer from the more common nonneovascular, or "dry," form of the disease. In the past few years, however, transplantation of human pluripotent stem cell-derived RPE (hPSC-RPE) has emerged as a promising new therapy for dry AMD. A Phase I clinical trial of human embryonic stem (hES)-derived RPE cells recently reported some preliminary encouraging results (2). Additionally, a Phase I trial that will use RPE cells generated from human induced pluripotent stem cells (hiPSCs) reprogrammed from the patients' own skin cells recently injected their first patient (3).

If the promise of hiPSC-based approaches for AMD is to be translated into the clinic, each patient would require individualized generation of RPE cells from his or her stem cells, thereby necessitating the development of simple, efficient, safe, and affordable protocols for RPE generation. Although highly efficient protocols have been established, they rely upon mixtures of growth factors (4–6) with the use of complex biologics derived from animal cells or bacteria, presenting potential clinical challenges. As an alternative approach, use of nonbiological products such as small molecules would limit the risk of infection or immune rejection (7). In addition, they offer a cost-effective alternative with less lot-to-lot variability. As a consequence, the development of small-molecule–based protocols has been the focus of extensive research (8). To date, however, the small-molecule–only protocols that have been developed for RPE differentiation have demonstrated only limited efficiency (9).

We report here development of a highly efficient, small-molecule–based protocol for the production of RPE from hPSC that is suitable for clinical application. We performed a quantitative real-time PCR (qPCR)-based high-throughput screen (HTS) for molecules that promote RPE differentiation, and complemented

Significance

Cell-based approaches utilizing retinal pigment epithelial (RPE)-like cells derived from human pluripotent stem cells (hPSCs) are being developed for the treatment of retinal degeneration. In most research published to date, the choice of the factors used to induce RPE differentiation is based on data from developmental studies. Here, we developed an unbiased approach directed at identifying novel RPE differentiation-promoting factors using a high-throughput quantitative PCR screen complemented by a novel orthogonal human induced pluripotent stem cell (hiPSC)-based RPE reporter assay. We identified chetomin, a dimeric epidithiodiketopiperazine, as a strong inducer of RPE; combination with nicotinamide resulted in efficient RPE differentiation. Single passage of the whole culture yielded a highly pure hPSC-RPE cell population that displayed many of the morphological, molecular, and functional characteristics of native RPE.

Author contributions: J.M., K.B., and D.J.Z. designed research; J.M., S.R.S., K.B., K.J.W., C.K., L.Z., and I.B. performed research; K.B., J.F., V.R., V.M.S., J.D., J.W., J.Q., B.C., S.T., R.D., and B.Z.O. contributed new reagents/analytic tools; J.M., S.R.S., J.F., K.J.W., C.A.B., C.K., J.W., J.Q., B.Z.O., I.B., G.A.L., and D.J.Z. analyzed data; and J.M., K.B., and D.J.Z. wrote the paper.

Conflict of interest statement: J.M., J.F., and D.J.Z. are coinventors on a patent application related to the use of chetomin for RPE differentiation (Differentiation of Human Pluripotent Stem Cells into Retinal Pigment Epithelium Using Chetomin; US Provisional Patent Application Serial No. 61/991,822).

This article is a PNAS Direct Submission.

[1]To whom correspondence should be addressed. Email: dzack@jhmi.edu.

This article contains supporting information online at www.pnas.org/lookup/suppl/doi:10.1073/pnas.1422818112/-/DCSupplemental.

the screen with a novel orthogonal hiPSC-based RPE reporter assay for compound validation. Using this strategy, we identified chetomin (CTM) as a potent promoter of RPE differentiation. Its use in combination with a previously known neural inducer, nicotinamide (NIC) (10, 11), provides a one-step treatment for differentiation of a wide range of hPSC lines. Following a single whole-dish passage, a pure and functional monolayer of RPE cells is obtained. This protocol should prove useful for the cost-efficient production of RPE cells.

Results

An RPE-Specific Tyrosinase Enhancer Drives Green Fluorescent Protein Expression in RPE Cells During hiPSC Differentiation into RPE. To follow RPE differentiation, we used a reporter hiPS cell line that expresses green fluorescent protein (GFP) specifically when the cells are differentiated into the RPE lineage (12). A GFP cassette was put under the control of an RPE-specific tyrosinase enhancer (Fig. 1*A*) (13) following a previously described approach (14). In mouse, we verified that this construct provided spatially and temporally restricted expression of GFP to RPE cells (Fig. 1 *B* and *C*). The tyrosinase enhancer–GFP construct (Tyr-GFP) was cloned into a lentiviral vector containing a red fluorescent protein (RFP) controlled by a constitutive Ubiquitin-C promoter (Fig. 1*D*). The construct was transduced into B42, a fibroblast-derived hiPS cell line (15), to generate the reporter line 3D1. In their undifferentiated, pluripotent state, 3D1 cells constitutively expressed RFP without evidence of GFP expression (Fig. 1*E*). After about 30 d of spontaneous differentiation, GFP expression was observed in colonies composed of pigmented cells whose morphology was reminiscent of RPE cells (Fig. 1*F*). To validate that GFP expression was indeed associated with RPE differentiation, fluorescence-activated cell sorting (FACS) was performed on the GFP-positive and -negative populations. Upon reseeding, FACS-sorted GFP-positive cells formed a confluent culture of GFP+/RFP+ cells, with a polygonal and pigmented morphology characteristic of RPE cells (Fig. 1 *G* and *H*). They also displayed higher expression of mature RPE markers compared with the GFP-negative cells (Fig. 1*I*). Together, these data show that GFP expression is specifically activated in cells committed to RPE fate during in vitro differentiation of Tyr-GFP 3D1 hiPSC.

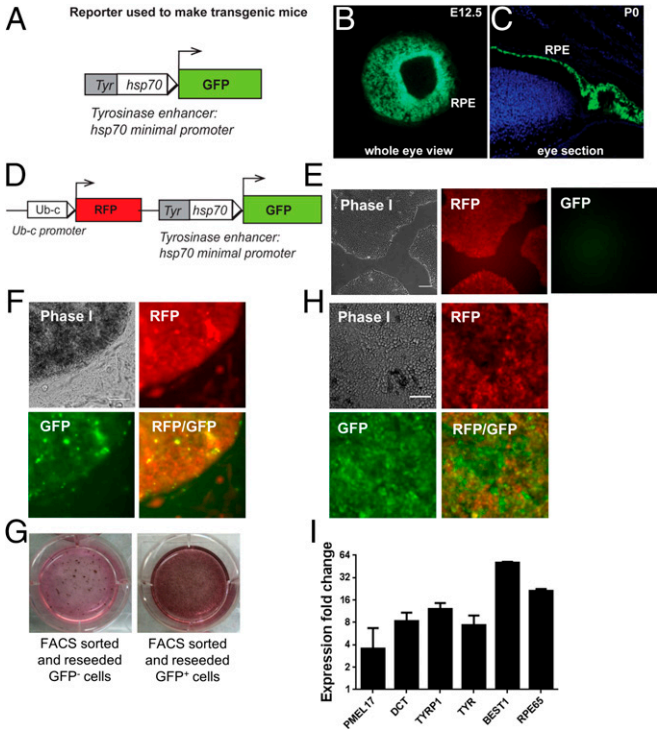

Fig. 1. Specific expression of a Tyr-GFP reporter in vivo, and in vitro during hiPSC differentiation. (*A*) Schematic of the GFP cassette under control of an RPE-specific enhancer (Tyr-GFP). (*B* and *C*) Tyr-GFP expression in vivo in the mouse eye. (*D*) Schematic of the Tyr-GFP:Ub-c-RFP construct. (*E*) Microscope images of 3D1 hiPSC in the pluripotent state. (*F*) Microscope images of 3D1 hiPSC during spontaneous RPE differentiation. (*G*) Morphology of Tyr-GFP 3D1 hiPSC after FACS and further culture for 1 mo. (*H*) Microscope images of 3D1 hiPSC-RPE. (*I*) RPE mature marker expression in sorted 3D1 hiPSC-RPE as measured by qPCR. Expression levels of GFP-positive sorted cells were normalized by expression levels of the GFP-negative cells. Error bars represent SD of biological replicates. BEST1, bestrophin 1; DCT, dopachrome tautomerase; PMEL17, premelanosome protein; RPE65, retinal pigment epithelium-specific protein, 65 kDa; TYR, tyrosinase; TYRP1, tyrosinase-related protein 1. [Scale bar: 40 μm (for all images in Fig. 1).]

High-Throughput qPCR Screen Identifies CTM as a Potent Inducer of RPE Differentiation. As our primary screen for RPE differentiation-promoting small molecules, we directly measured endogenous RPE marker expression using high-throughput qPCR (HT qPCR). Tyr-GFP 3D1 hiPSCs were seeded in 384-well plates and treated for 10 d with four different concentrations of molecules from a focused library of 303 compounds (StemSelect; Millipore) (*SI Materials and Methods* and Table S1). Cells were then cultured for 5 d in differentiation medium (DM) to allow for higher marker expression levels to be achieved, and then expression of three RPE markers [microphthalmia-associated transcription factor (MITF), orthodenticle homeobox 2 (OTX2), and premelanosome protein (PMEL17)] was assessed by qPCR (Fig. 2*A*). The transcription factors MITF and OTX2 are both required for RPE differentiation, whereas PMEL17 is a matrix protein present in the melanosome precursors of pigmenting cells. Only one of the compounds tested, CTM, was found to consistently up-regulate all three RPE markers: 40 nM CTM increased the expression of the markers 9- to 15-fold compared with DMSO-treated controls (Fig. 2*B*), whereas higher concentrations of CTM caused marked cell death. CTM is a dimeric epidithiodiketopiperazine (ETP) metabolite of the fungus *Chaetomium cochliodes* and *Chaetomium seminudum* species (Fig. 2*C*).

Next, we validated the ability of CTM to induce RPE marker expression in four different hPSC lines. Following the protocol of the primary screen, cells were cultured in the presence of CTM from day 0 to day 10 at concentrations ranging from 1.25 to 80 nM in twofold increments. About a week after initiation of CTM treatment, a high level of cell death was observed above 20 nM CTM in the hESC lines H7 and H9, whereas the hiPSC lines IMR904 and 3D1 tolerated up to 40 and 80 nM CTM, respectively. Although the dose–response curves differed, all three markers were up-regulated by CTM in a dose-dependent pattern in all four hPSC lines (Fig. 2*D*). These results confirm the HT qPCR data and indicate that CTM's effect on RPE marker expression is not limited to the specific cell line used in the screen.

To further validate CTM's effect on RPE differentiation in an orthogonal assay, 3D1 hiPSC were treated with 10–80 nM CTM for 10 d, and flow-cytometric analysis of Tyr-GFP expression was performed at day 35. The percentage of Tyr-GFP+ cells followed a dose-dependent pattern, with a plateau above 40% positive cells for 40–80 nM CTM compared with about 15% in control ($P < 10^{-4}$ by ANOVA) (Fig. 2 *E* and *F*). We repeated the dose–response experiments and assessed the extent of RPE differentiation by immunostaining for PMEL17 followed by flow cytometry (Fig. 2*G*). Control conditions yielded 10–15% PMEL17+ cells after 35 d of differentiation, whereas treatment with 20 nM CTM increased the percentage to 30% for H7 and H9 cells, and treatment with 40 nM CTM increased efficiency to ∼40% for IMR904 and 3D1 cells ($P < 0.05$ by ANOVA for all four hPSC lines) (Fig. 2*H*), demonstrating that the differentiation efficiency is increased threefold to fourfold by CTM treatment.

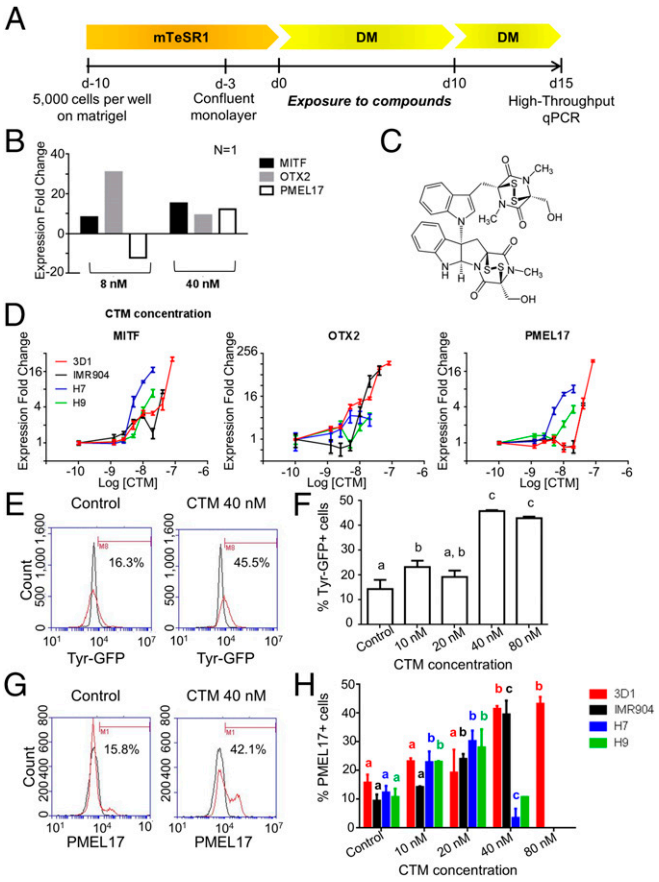

Fig. 2. Identification and validation of CTM as a promoter of RPE differentiation. (*A*) Schematic of the HT qPCR screening strategy. (*B*) RPE marker expression in wells treated with CTM (n = 1 for each concentration). Expression levels were normalized by mean of DMSO-treated samples using the ΔΔCt method. (*C*) Chemical structure of CTM. (*D*) RPE marker expression at day 15 following CTM treatment in four different hPSC lines, as measured by qPCR. Data were normalized by the expression levels in control conditions. (*E*) Flow-cytometric analysis of the expression of Tyr-GFP at day 35 in control and CTM-treated samples (red). 3D1 hiPSC in the pluripotent state were used as a negative control (black). (*F*) Expression of Tyr-GFP at day 35 following CTM treatment, as measured by flow cytometry. (*G*) Flow-cytometric analysis of the expression of PMEL17 at day 35 in control and CTM-treated samples (red). The isotype control is displayed in black. (*H*) Expression of PMEL17 at day 35 following CTM treatment, as measured by flow cytometry in four different hPSC lines. For each hPSC line, differing letters indicate statistically significant mean differences ($P < 0.05$ by ANOVA). In all cases, error bars represent SD of three biological replicates.

Despite the presence of large areas of PMEL17+ cells at day 15, and Tyr-GFP+ cells at day 30 of differentiation (Fig. S1 *A* and *B*), we surprisingly did not see pigmented clusters in the CTM-treated cultures, although they were readily apparent in the control wells (Fig. S1*C*). To assess whether the Tyr-GFP+ cells obtained after CTM treatment were indeed bona fide RPE cells, the whole culture was passaged onto a new dish and grown in RPE medium (RPEM) (*Materials and Methods*). During the next month, cells grew into a confluent monolayer made of pigmented and polygonal cells (Fig. S1*D*), a morphology characteristic of RPE cells. They also homogeneously expressed the RPE markers MITF and the tight junction protein ZO-1 (Fig. S1*D*), and ∼95% were Tyr-GFP+ (Fig. S1 *D* and *E*). On the contrary, when control cultures were passaged into RPEM, they failed to grow into a homogenous pigmented monolayer, and instead formed pigmented clusters surrounded by fibroblast looking cells, as previously described (16). These results demonstrate that CTM is a potent and reproducible inducer of RPE differentiation.

Disruption of the CH1 Domain of p300 Is Not the Main or Only Mechanism Involved in CTM-Induced RPE Differentiation. CTM has known antimicrobial activity (17) and is a disruptor of the CH1 domain of the p300 coactivator (18). To test whether CTM's RPE-inducing activity was related to its effect on p300, we assessed the ability of ETP2, another dimeric ETP compound (Fig. S2*A*) that binds the CH1 domain with high affinity, to induce RPE differentiation in hPSC. Dose–response treatment of 3D1 hiPSC with ETP2 for 10 d was followed by qPCR at day 15. Massive cell death was observed with ETP2 at 50 nM and above. MITF and OTX2 were both significantly up-regulated upon ETP2 treatment, although their respective peak increase was reached at different concentrations (Fig. S2*B*). On the other hand, PMEL17, a more mature RPE marker, did not show any significant change in expression with ETP2 treatment.

We further assessed the extent of RPE differentiation following ETP2 treatment by analyzing Tyr-GFP expression at day 35 by flow cytometry (Fig. S2*C*). We did not observe any statistically significant change between control and ETP2-treated samples ($P > 0.27$ by ANOVA). Interestingly, pigmented colonies were not observed above 6 nM ETP2. These results suggest that CTM's differentiation-promoting activity, such as RPE lineage induction or initiation of early differentiation, may be due in part to CH1 domain disruption, whereas the ability to promote more mature RPE differentiation requires an activity in addition to CH1 domain disruption.

To gain a better understanding of CTM action at a broader level, hPSC-derived embryoid bodies were grown for 15 d in the presence or absence of 50 nM CTM, followed by qPCR for key markers of the primordial lineages (Fig. S2*D*). Although neuroectodermal markers (PAX6 and OTX2) were up-regulated, as might be expected based on our earlier results, CTM also strongly inhibited expression of markers of the mesodermal and endodermal fates ($P < 0.05$ by multiple T test). These results indicate that CTM's mechanism of action might be quite complex and multifactorial, as it induces neuroectodermal differentiation while actively repressing alternative cell fates.

NIC Prevents Excessive Cell Death During CTM-Induced RPE Differentiation. We next tested different lengths of time for CTM treatment and found that expression of key RPE markers was optimal when CTM was added during the first 2 wk of differentiation.

Importantly, while performing these experiments, we observed significant cell death of H7 cells with CTM treatment length of 2 wk and above. CTM cellular toxicity has been described previously (18). In sensitive hPSC lines, such as H7, we observed patches of differentiating cells after 2-wk CTM treatment at 25 nM, whereas there was only minimal cell survival at 50 nM. On the contrary, in less sensitive lines, such as 3D1, cells formed a confluent monolayer regardless of the culture conditions. These observations were quantified by counting the remaining live cells by flow cytometry, after 2-wk CTM treatment (Fig. S3). Apoptotic and dead cells were excluded from the analysis based on SytoxRed staining. As NIC has been reported to protect hPSC from cell death during neuroectoderm differentiation through PARP1 inhibition (11), we tested whether it could reduce CTM-induced cell death. Cotreatment with 10 mM NIC prevented cell loss in H7 at 50 nM CTM, and cotreatment with NIC more than doubled the number of live 3D1 cells when 50 nM CTM was used (Fig. S3). Overall, CTM cellular toxicity can be prevented by combination with NIC, so confluent cell monolayers can be maintained throughout hPSC differentiation.

Combined Small-Molecule Treatment Followed by Culture in RPEM Leads to High-Efficiency Generation of RPE Cells with Characteristic Morphology. Although CTM, or CTM plus NIC, treatment led to RPE induction as measured by marker expression and Tyr-GFP reporter activation, surprisingly pigmented colonies were not readily observed (Fig. S1*B* and Fig. 3*A*). We previously showed that, after passage in RPEM, a medium originally designed for fetal RPE

culture, CTM-induced RPE cells were able to acquire characteristic RPE morphology. Therefore, we decided to test whether growing differentiating hPSC in RPEM would promote RPE pigmentation. After 2-wk induction with CTM and NIC in DM, hPSC were switched to RPEM (Tables S2 and S3). Within 1–2 wk of switching to RPEM, pigmented clusters started to become visible, and by the third week they covered the majority of the well surface (Fig. 3*A*). For cultures switched to RPEM, robust Tyr-GFP expression was observed in colonies with polygonal and pigmented cells, whereas for cells maintained in DM, there was no perceptible change in morphology despite Tyr-GFP activation (Fig. 3*B*). Flow cytometry was used to quantify the effect of RPEM on Tyr-GFP expression. Cells cultured in RPEM showed higher levels of Tyr-GFP expression (Fig. 3*C*), with a 24% increase in median fluorescent index (MFI) for the whole population compared with cells maintained in DM ($P = 0.02$, t test) (Fig. 3*D*). The percentage of Tyr-GFP+ cells was moderately increased, from 55.6% (±5.5%) for hiPSC differentiated in DM to 63.9% (±5.4%) for their counterparts grown in RPEM ($P = 0.04$, t test). Altogether, these results indicate that switching to RPEM following cotreatment with CTM and NIC both promotes RPE morphology and increases differentiation efficiency.

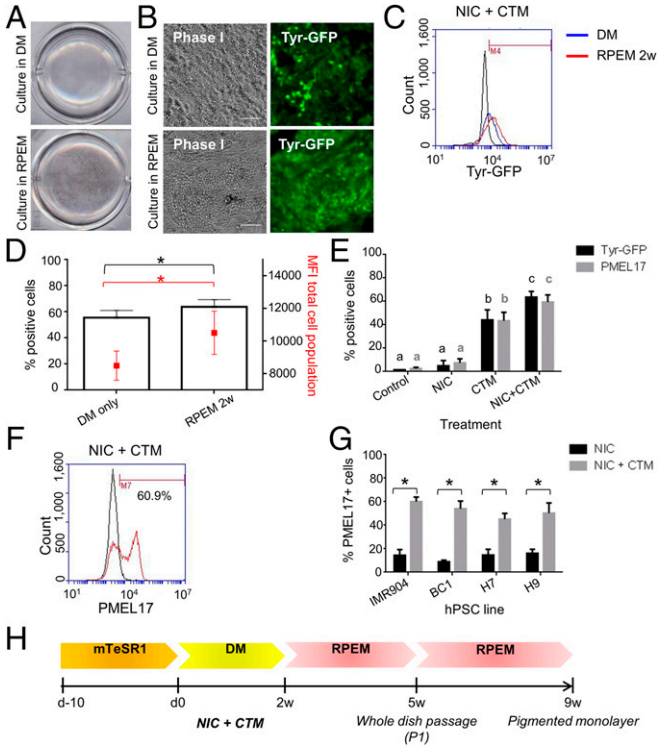

Fig. 3. Differentiation of hPSC into RPE following treatment with combination of CTM and NIC. (*A* and *B*) Morphology of differentiating hPSC at day 35 in DM vs. RPEM, with *A* showing macroscopic and *B* showing microscopic images. (Scale bar: 40 μm.) (*C*) Flow-cytometric analysis of Tyr-GFP expression at day 35 after culture in DM or RPEM. 3D1 hiPSC in the pluripotent state were used as a negative control (black). (*D*) Histogram displaying the percentage of Tyr-GFP+ cells and the median fluorescent intensity (MFI) of the whole cell population in 3D1 hiPSC. (*E*) Expression of RPE markers at day 35, as measured by flow cytometry in 3D1 hiPSC. (*F*) Flow-cytometric analysis of PMEL17 expression at day 35 in hPSCs cultured in RPEM (red). The isotype control is displayed in black. (*G*) Expression of PMEL17 at day 35 in four different hPSC lines, as assessed by flow cytometry. The difference between NIC and NIC plus CTM is statistically significant by T test ($P < 0.001$ for all four hPSC lines). (*H*) Schematic of hPSC differentiation into RPE using combination of NIC and CTM, followed by culture in RPEM. RPE purification is achieved at day 35 by whole-dish passage (P1). Error bars represent SD of three biological replicates.

In a parallel set of experiments, we observed that switching to RPEM after 2 wk of CTM treatment also led to the emergence of pigmented colonies at 35-d differentiation (data not shown). However, the percentages of both Tyr-GFP+ and PMEL17+ cells were significantly lower ($P < 0.0054$ for Tyr-GFP, $P < 0.0026$ for PMEL17) compared with cotreatment with CTM and NIC (Fig. 3*E*). Thus, the addition of NIC to CTM also helps further improve RPE generation efficiency, in agreement with recent studies on its role during RPE differentiation (6, 10).

Compared with control and NIC alone, cultures treated with CTM or with a combination of CTM and NIC showed a strong induction of the eye field transcription factor paired box gene 6 (PAX6) and MITF, whereas OTX2 expression was maintained at higher levels throughout the first month of differentiation (Fig. S4). As a presumed consequence of the strong up-regulation of RPE-inducing transcription factors (14), PMEL17 expression was dramatically increased after the second week. Compared with NIC alone, tyrosinase (TYR), which encodes the enzyme responsible for the conversion of tyrosine to pigment melanin, also displayed sixfold up-regulation by the fourth week of differentiation in cultures treated with CTM alone, or cotreated with CTM and NIC. This is consistent with the extended area of pigmented cells observed in cultures treated with CTM and NIC.

Finally, we validated our optimized approach for RPE differentiation (Fig. 3*H*) on four additional hPSC lines. All four lines responded to the protocol by yielding RPE cells with efficiencies ranging from 45% to 60% of PMEL17+ cells at day 35 (Fig. 3 *F* and *G*). Altogether, these data show that during CTM-plus-NIC–directed differentiation, RPE markers are strongly up-regulated. As a consequence, high yields of RPE cells are obtained from a wide range of hPSC lines.

Pure, Polarized, and Functional RPE Monolayers Are Obtained After a Single Whole-Dish Passage. After 2-wk cotreatment with CTM and NIC in DM, differentiating hPSC lines 3D1, IMR904, and H7 were switched to RPEM. At day 35, whole cultures were dissociated to single cells, passaged at high density (P1), and cultured in RPEM (Fig. 3*H*). A month later, the 3D1 culture had grown into a monolayer of pigmented and polygonal cells, and displayed a majority of Tyr-GFP–expressing cells (Fig. 4*A* and Fig. S5*A*). Domes had also formed (Fig. S5*B*), suggesting that the cells were functional and actively transporting fluid, as is known to occur in mature, tight junction-bearing, RPE cells (1). Key RPE markers such as MITF, PMEL17, and the tight junction protein ZO-1 were strongly expressed in all three tested hPSC lines (Fig. 4*B*). When hPSC-RPE cells were left to mature for another month, they also expressed the chloride channel-related protein Bestrophin 1 (BEST1), as well as retinaldehyde-binding protein 1 (RLBP1) and retinal pigment epithelium-specific protein of 65 kDa (RPE65), both proteins involved in the visual cycle (Fig. 5*B*). Additionally, the cells show the polarity expected of RPE cells, with ZO-1 and BEST1 showing apical (Fig. 4*C*) and basolateral (Fig. 4*D*) localization (19, 20). Quantification of marker expression by flow cytometry indicated that the hPSC-RPE cultures were highly pure: 95.1–98.6% MITF+, 92.6–98.3% PMEL17+, and >95% Tyr-GFP+ (Fig. 4 *E*–*G* and Table S4).

Next, we tested the phagocytosis of photoreceptor outer segments (POS), which is an essential function assumed by RPE in vivo (1). hPSC-RPE cells were incubated in the presence of FITC-labeled POS for 5 h. Free POS were washed away and external fluorescence was quenched with trypan blue to visualize internalized POS, whereas ZO-1 staining marked the apical side. Apically localized POS were extensively observed within hPSC-RPE layers (Fig. 4*I*). Flow cytometry analysis (21) indicated that 66.7–71.4% of hPSC-RPE cells had phagocytosed POS (Fig. 4*H* and Table S4). RPE cells in vivo are also known to secrete preferentially vascular endothelial growth factor (VEGF) and pigment epithelium-derived factor (PEDF) to the basal and apical side, respectively (1). We

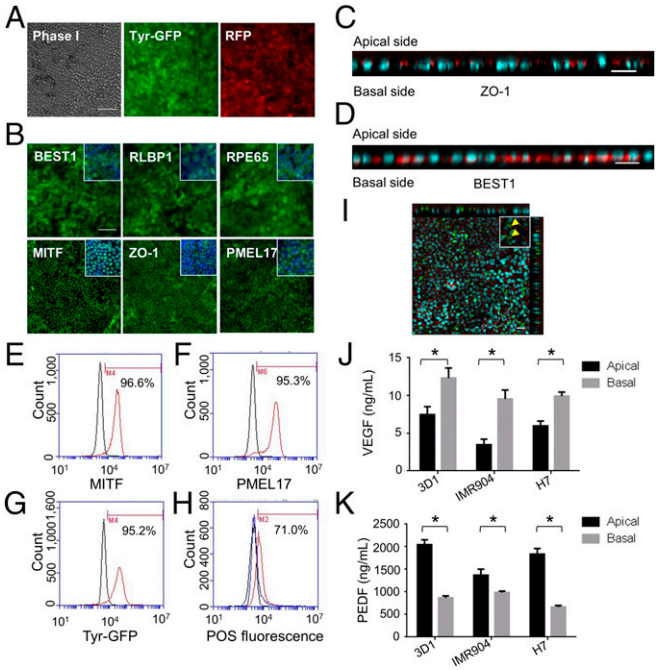

Fig. 4. Characterization of hPSC-RPE obtained after NIC-plus-CTM induction. (*A*) Microscope images of 3D1 hiPSC-RPE. (Scale bar: 40 μm.) (*B*) Microscope images of IMR90-4–derived hPSC-RPE immunostained for key RPE markers. *Insets* display higher magnification of the images with Hoechst (blue) counterstaining. (Scale bar: 40 μm.) Immunostaining of the top three panels was performed on hPSC-RPE cultured for 60 d after P1, whereas the bottom three panels were obtained following 30 d culture after P1. (*C* and *D*) *Z*-stack confocal micrographs showing typical polarized expression of RPE proteins, with ZO-1 (red) demonstrating apical localization (*C*) and BEST1 (red) demonstrating basolateral localization (*D*). The nuclei were counterstained with Hoechst (cyan). (Scale bars: 20 μm.) (*E*–*G*) Flow-cytometric analysis of the expression of RPE markers in hPSC-RPE 1 mo after purification by whole-dish passage. The profile of cells stained with RPE marker antibodies is shown in red, and the isotype control is displayed in black. (*H*) Flow-cytometric analysis of hPSC-RPE cells phagocytosis. The profile of hPSC-RPE incubated with photoreceptor outer segment (POS) is shown in red. The no-POS control is displayed in black, whereas POS internalization was specifically blocked with an anti-integrin $\alpha_V\beta_5$ antibody in the control shown in blue. (*I*) Confocal microphotograph showing phagocytosis of POS (green) by IMR90-4–derived hPSC RPE. The apical sides of hPSC-RPE cells are stained with ZO-1 (red), whereas nuclei are counterstained with Hoechst (cyan). (Scale bar: 20 μm.) *Inset* shows a higher magnification with yellow arrows pointing at phagocytosed POS. (*J*) Polarized secretion of VEGF-A from the apical and basal sides of hPSC-RPE cells grown on Transwells. (*K*) Polarized secretion of PEDF from the apical and basal sides of hPSC-RPE cells grown on Transwells. For both *J* and *K*, the difference between apical and basal secretion is statistically significant by *t* test ($P < 0.01$ for all three hPSC lines). In all cases, error bars represent SD of three biological replicates.

therefore grew hPSC-RPE cells on Transwells and collected medium from the upper and lower reservoirs. VEGF was preferentially found in the lower reservoir, reflecting basal secretion (Fig. 4*J*), whereas PEDF secretion was predominant in the upper reservoir, reflecting apical secretion (Fig. 4*K*). This polarized pattern of growth factor secretion is in accordance with previous studies using native RPE and hPSC-RPE (19, 22). Taken together, these results demonstrate that, following small-molecule–directed differentiation of hPSC, a polarized and functional monolayer of hPSC-RPE showing a high degree of cell purity is obtained from a single whole-dish passage.

Directed RPE Differentiation Is Clinically Relevant. To increase the clinical relevance of our small-molecule–only approach for RPE differentiation, we adapted it to a completely defined and xeno-free process: 3D1 hiPSCs were differentiated with NIC and CTM on synthetic vitronectine peptide-acrylate surfaces using xeno-free versions of B27 and KnockOut serum (*Supporting Information*). This process yielded over 60% (64.1 ± 3.8%) Tyr-GFP+ cells after 1 mo of differentiation (Fig. S6*A*), whereas high-purity RPE monolayers (95.6 ± 0.4% PMEL17+, 95.9 ± 0.1% Tyr-GFP+) expressing key markers were obtained following a single passage (Fig. S6 *B*–*D*). Additionally, after verifying that they had a normal karyotype (Fig. S7), 3D1 hPSC-RPE cells at P1 were injected into the subretinal space of albino, NOD-SCID mice. Fundus imaging taken 2 wk later displayed the presence of numerous pigmented clusters in the injection area, suggesting that the injected cells had survived the transplantation process and maintained their RPE phenotype in vivo (Fig. S8*A*). Retinal section confirmed this observation showing RFP- and GFP-positive cells, integrated within the host RPE layer (Fig. S8*B*). The presence of rhodopsin-positive fragments within the RFP-positive cytoplasmic compartment of hiPSC-RPE cells suggests that these cells were functional and phagocytosed POS from the endogenous photoreceptor cells (Fig. 5, arrowheads). Significantly, we did not detect any cellular overgrowth that would have been suggestive of tumor formation in any of the injected animals ($n = 8$ injected eyes).

Discussion

In most studies reported to date, directed differentiation of hPSC into RPE is induced, at least in part, by the use of growth factor and related molecules that recapitulate in vivo developmental cues. In this report, we used a discovery-based HTS approach to identify small molecules that promote RPE generation and differentiation. Fluorescence-based HTS have been successfully developed in previous studies to identify compounds directing hPSC differentiation toward a number of lineages (23). However, fluorescence-based HTS are prone to false-positive hits. Sources of apparent activity in such assays include fluorescent compounds and impurities that may have been present in the chemical sample (24) as well as autofluorescence of apoptotic/dead cells. Perhaps reflecting these issues, when we performed preliminary screens using high-throughput flow cytometry to assess the expression of Tyr-GFP in 3D1 hiPSCs treated with small-molecule libraries, we were unable to validate any of the nine primary hits obtained out of almost 1,000 compounds tested. Compared with a fluorescence-based reporter system, qPCR directly measures native mRNA expression levels, which limits artifacts that can cause false discovery. The Tyr-GFP 3D1 hiPSC line then proved useful as an orthogonal assay to validate the primary hits from the qPCR screen. HT qPCR screening has been used successfully in a previous study with mouse embryonic stem cells

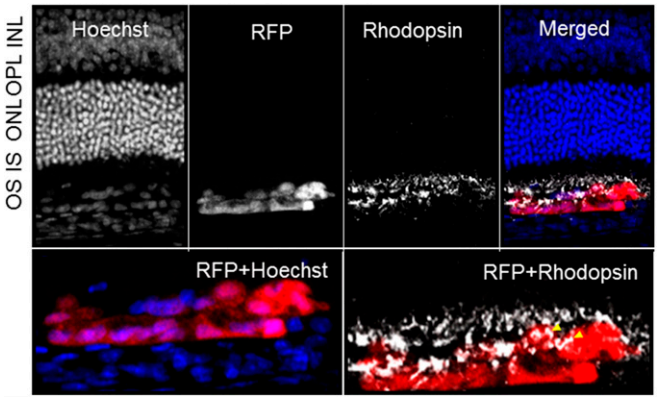

Fig. 5. Transplantation of 3D1 hiPSC-RPE into the subretinal space of NOD-SCID albino mice. Confocal micrograph showing the presence of rhodopsin-positive fragments (yellow arrowheads) 2 wk posttransplantation within the RFP-positive cytoplasmic compartment of injected 3D1 hiPSC-RPE.

(25); however, to the best of our knowledge, this is the first report of its application in the context of hPSC differentiation.

Following the above-described approach, we performed a pilot screen on a focused library of about 300 compounds. Despite the small size of this library, we identified CTM as a novel and potent promoter of RPE differentiation. Protocol optimization, with the addition of NIC to CTM, led to high yields of RPE cells after 1 mo of differentiation. A pure and functional RPE monolayer was obtained from a single whole-dish passage. This is an improvement over our previous approach based on low-efficiency spontaneous differentiation, for which two rounds of whole-dish passages were necessary to obtain a pure RPE population (16). Although high-efficiency RPE differentiation protocols have been reported, with yields as high as 60–97%, these high-efficiency approaches all involve the addition of growth factors that are suboptimal for clinical use (4, 6), or were tested on only a limited number of hESC lines (5). A small-molecule–only differentiation protocol has been reported, but yield and efficacy were limited, with 26% of colonies showing pigmented cells after 2 mo of differentiation (9). For a common hiPSC line, IMR904, our small-molecule–only approach is comparable to the best growth factor-based protocol published to date (6). To test the reproducibility of our protocol, the hiPSC line BC1 (26), which had never been cultured in our hands, was amplified by clonal propagation for two passages before beginning our RPE differentiation protocol. The fact that it generated RPE cells as efficiently as the other hPSC lines suggests that our protocol should be readily implementable in other laboratories and with a variety of ESCs and patient-derived iPSCs.

A striking observation made during CTM-directed, or CTM- and NIC-directed, differentiation into RPE was the absence of pigmented colonies when cultures were maintained in DM, whereas pigmented cells were readily observed in control and NIC-only conditions. In the light of these results, it is advisable to remain cautious with the use of pigmented colonies to determine RPE differentiation, as we have demonstrated that RPE-committed cells can exist in a culture without showing pigmentation or RPE-specific morphology. Interestingly, a simple medium change was sufficient to induce the acquisition of hallmarks of pigmentation and RPE morphology in cultures treated with small molecules, suggesting that CTM-committed RPE cells are not fully mature in DM and require RPEM to acquire their characteristic morphology.

Finally, we observed that during optic vesicle formation from hPSC (27), CTM treatment seems to increase the number of neuronal folds, suggesting a possibly wider role for this compound in retinal differentiation.

Materials and Methods

Differentiation and Culture of RPE from hPSC. A detailed version of the optimized differentiation protocol and other methods can be found in *Supporting Information*. Briefly, hPSCs were seeded at 20,000 cells per cm^2 on Matrigel and grown in mTeSR1 in a 10% CO_2/5% O_2 incubator for 5 d. Afterward, they were transferred to a 5% CO_2/20% O_2 incubator and cultured for 5 additional days. At this point, culture medium was switched to DM, and in some experiments supplemented with 10 mM NIC and/or CTM (Sigma) at concentrations ranging from 1.25 to 80 nM. After 10–15 d, cells were maintained in DM only for 3 more weeks, or switched to RPEM. Differentiated cells were dissociated in Accumax (Sigma), plated at 250–300,000 cells per cm^2 and grown in RPEM. All surgical and animal care procedures were performed in compliance with the Animal Care and Use Committee of the Johns Hopkins University School of Medicine and the Association for Research in Vision and Ophthalmology statement on the Use of Animals.

ACKNOWLEDGMENTS. We thank Dr. Linzhao Cheng (The Johns Hopkins University) for providing hiPSC BC1, and Dr. Emeline Nandrot (Institut de la Vision) for providing FITC-POS. This work was supported by grants from Foundation Fighting Blindness Wynn-Gund Translational Acceleration Program, Bright Focus Macular Degeneration Research Program, NIH Grants 5R21EY023812-02 and P30EY001765, unrestricted funds from Research to Prevent Blindness, Inc., and generous gifts from the Guerrieri Family Foundation, Mr. and Mrs. Robert and Clarice Smith, and the Raab Family Foundation.

1. Strauss O (2005) The retinal pigment epithelium in visual function. *Physiol Rev* 85(3):845–881.
2. Schwartz SD, et al. (2015) Human embryonic stem cell-derived retinal pigment epithelium in patients with age-related macular degeneration and Stargardt's macular dystrophy: Follow-up of two open-label phase 1/2 studies. *Lancet* 385(9967):509–516.
3. Cyranoski D (2014) Japanese woman is first recipient of next-generation stem cells. *Nature*, 10.1038/nature.2014.15915.
4. Zahabi A, et al. (2012) A new efficient protocol for directed differentiation of retinal pigmented epithelial cells from normal and retinal disease induced pluripotent stem cells. *Stem Cells Dev* 21(12):2262–2272.
5. Leach LL, Buchholz DE, Nadar VP, Lowenstein SE, Clegg DO (2015) Canonical/β-catenin Wnt pathway activation improves retinal pigmented epithelium derivation from human embryonic stem cells. *Invest Ophthalmol Vis Sci* 56(2):1002–1013.
6. Buchholz DE, et al. (2013) Rapid and efficient directed differentiation of human pluripotent stem cells into retinal pigmented epithelium. *Stem Cells Transl Med* 2(5):384–393.
7. Klimanskaya I, Rosenthal N, Lanza R (2008) Derive and conquer: Sourcing and differentiating stem cells for therapeutic applications. *Nat Rev Drug Discov* 7(2):131–142.
8. Xu T, Zhang M, Laurent T, Xie M, Ding S (2013) Concise review: Chemical approaches for modulating lineage-specific stem cells and progenitors. *Stem Cells Transl Med* 2(5):355–361.
9. Osakada F, et al. (2009) In vitro differentiation of retinal cells from human pluripotent stem cells by small-molecule induction. *J Cell Sci* 122(Pt 17):3169–3179.
10. Idelson M, et al. (2009) Directed differentiation of human embryonic stem cells into functional retinal pigment epithelium cells. *Cell Stem Cell* 5(4):396–408.
11. Cimadamore F, et al. (2009) Nicotinamide rescues human embryonic stem cell-derived neuroectoderm from parthanatic cell death. *Stem Cells* 27(8):1772–1781.
12. Bharti K, Davis J, Corneo B, Temple S, Miller S (2012) Use of an iPS reporter cell line expressing RPE-specific GFP for improving iPS cell to RPE differentiation. *Invest Ophthalmol Vis Sci* 53(6):Poster Abstract 2691.
13. Murisier F, Guichard S, Beermann F (2007) Distinct distal regulatory elements control tyrosinase expression in melanocytes and the retinal pigment epithelium. *Dev Biol* 303(2):838–847.
14. Bharti K, et al. (2012) A regulatory loop involving PAX6, MITF, and WNT signaling controls retinal pigment epithelium development. *PLoS Genet* 8(7):e1002757.
15. Ferrer M, et al. (2014) A multiplex high-throughput gene expression assay to simultaneously detect disease and functional markers in induced pluripotent stem cell-derived retinal pigment epithelium. *Stem Cells Transl Med* 3(8):911–922.
16. Maruotti J, et al. (2013) A simple and scalable process for the differentiation of retinal pigment epithelium from human pluripotent stem cells. *Stem Cells Transl Med* 2(5):341–354.
17. Brewer D, et al. (1972) Ovine ill-thrift in Nova Scotia. 5. The production and toxicology of chetomin, a metabolite of *Chaetomium* spp. *Can J Microbiol* 18(7):1129–1137.
18. Kung AL, et al. (2004) Small molecule blockade of transcriptional coactivation of the hypoxia-inducible factor pathway. *Cancer Cell* 6(1):33–43.
19. Maminishkis A, et al. (2006) Confluent monolayers of cultured human fetal retinal pigment epithelium exhibit morphology and physiology of native tissue. *Invest Ophthalmol Vis Sci* 47(8):3612–3624.
20. Marmorstein AD, et al. (2000) Bestrophin, the product of the Best vitelliform macular dystrophy gene (VMD2), localizes to the basolateral plasma membrane of the retinal pigment epithelium. *Proc Natl Acad Sci USA* 97(23):12758–12763.
21. Westenskow PD, et al. (2012) Using flow cytometry to compare the dynamics of photoreceptor outer segment phagocytosis in iPS-derived RPE cells. *Invest Ophthalmol Vis Sci* 53(10):6282–6290.
22. Kokkinaki M, Sahibzada N, Golestaneh N (2011) Human induced pluripotent stem-derived retinal pigment epithelium (RPE) cells exhibit ion transport, membrane potential, polarized vascular endothelial growth factor secretion, and gene expression pattern similar to native RPE. *Stem Cells* 29:825–835.
23. Li W, Jiang K, Wei W, Shi Y, Ding S (2013) Chemical approaches to studying stem cell biology. *Cell Res* 23(1):81–91.
24. Thorne N, Auld DS, Inglese J (2010) Apparent activity in high-throughput screening: Origins of compound-dependent assay interference. *Curr Opin Chem Biol* 14(3):315–324.
25. Dykhuizen EC, Carmody LC, Tolliday N, Crabtree GR, Palmer MA (2012) Screening for inhibitors of an essential chromatin remodeler in mouse embryonic stem cells by monitoring transcriptional regulation. *J Biomol Screen* 17(9):1221–1230.
26. Chou BK, et al. (2011) Efficient human iPS cell derivation by a non-integrating plasmid from blood cells with unique epigenetic and gene expression signatures. *Cell Res* 21(3):518–529.
27. Reichman S, et al. (2014) From confluent human iPS cells to self-forming neural retina and retinal pigmented epithelium. *Proc Natl Acad Sci USA* 111(23):8518–8523.
28. Synnergren J, et al. (2007) Differentiating human embryonic stem cells express a unique housekeeping gene signature. *Stem Cells* 25(2):473–480.
29. Meyer JS, et al. (2009) Modeling early retinal development with human embryonic and induced pluripotent stem cells. *Proc Natl Acad Sci USA* 106(39):16698–16703.
30. Gamm DM, et al. (2008) A novel serum-free method for culturing human prenatal retinal pigment epithelial cells. *Invest Ophthalmol Vis Sci* 49(2):788–799.